Electronic Supplementary Information for

Effects of Phosphate on Biotite Dissolution and Secondary Precipitation: Implications for Geologic CO₂ Sequestration

Lijie Zhang[1], Doyoon Kim[1], Yongman Kim[2], Jiamin Wan[2], and Young-Shin Jun[1], *

[1]*Department of Energy, Environmental and Chemical Engineering, Washington University,*

St. Louis, MO 63130

[2]*Energy Geosciences Division, Lawrence Berkeley National Laboratory, Berkeley, CA 94720*

Address: One Brookings Drive, Campus Box 1180

E-mail: ysjun@seas.wustl.edu

Phone: (314)935-4539

Fax: (314)935-7211

http://encl.engineering.wustl.edu/

Physical Chemistry Chemical Physics

*To Whom Correspondence Should Be Addressed

Summary

Sixteen pages, including ten figures and three tables.

S1. Model mica mineral biotite

To prepare biotite particles for ATR experiments, clean biotite flakes were first ground in a grinder with stainless steel blades in dry condition for half an hour, and then particles in the size range of 53–106 μm were collected with sieves. The biotite particles were sonicated in ethanol for half an hour to detach tiny particles, and the suspension was allowed to settle for 3 hours. The supernatant was collected and the size of the particles was measured by dynamic light scattering as around 100 nm. The time periods for sonication and settlement were tried many times to get the final particle size to be around 100 nm.

Table S1 Chemical composition of biotite used in this study, analyzed with X-ray fluorescence (XRF) (unit: wt%).

	SiO_2	Al_2O_3	FeO	MgO	TiO_2	MnO	K_2O	Na_2O	CaO	Others (H, F)
XRF	39.0	11.1	17.5	13.9	2.19	0.84	9.4	0.6	0.1	5.37

Chemical formula: $K_{0.91}Na_{0.08}Ca_{0.05}Mg_{1.72}Mn_{0.06}Fe_{1.12}Ti_{0.12}Al_{1.00}Si_{2.98}O_{10}(F_{0.51}(OH)_{0.49})_2$

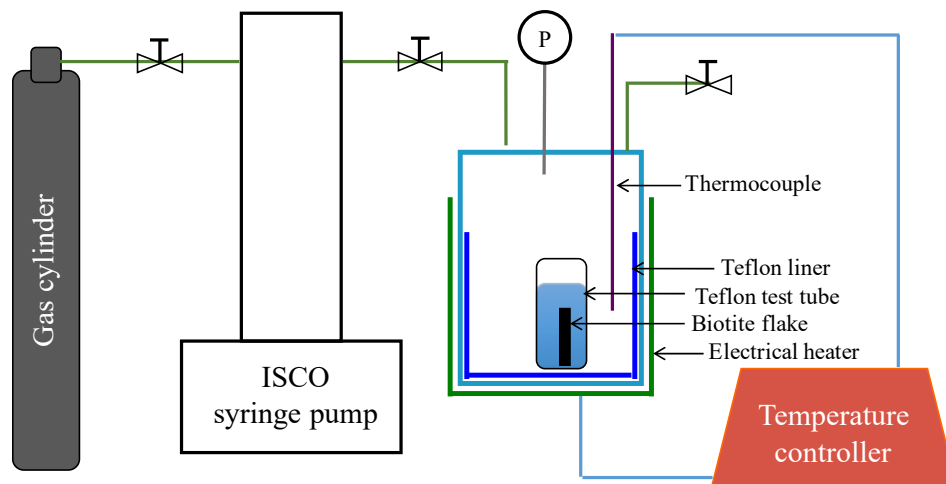## S2. High temperature and high pressure batch experiments

Figure S1 Experimental setup for the high temperature and high pressure batch experiments.

High temperature and high pressure experiments:

Biotite samples were reacted in prepared solutions in a high temperature and high pressure reactor (Figure S1). First, one piece of clean biotite flake was placed in a PTFE tube containing 4 mL of prepared solutions. The tube was covered with Teflon tape with two small holes in the tape to allow supercritical CO_2 ($scCO_2$) to diffuse into the tube. Triplicate samples were prepared and placed in the 300 mL Teflon liner, which was located inside the reactor. The temperature of the reactor was maintained at 95 °C by a temperature controller. CO_2 was injected into the reactor by a syringe pump and controlled at 102 atm. The reactions were allowed to proceed for desired time periods (3, 8, 22, 44, 70, and 96 h).

After high P/T experiments, the reactor was taken out from the heating mantle and allowed to cool down. Meanwhile, the reactor was slowly degassed by releasing the pressure valve. The degassing process took about 0.5 h. Then the samples were taken out from the reactor and collected for further characterizations. The whole process was controlled to be same for different reaction conditions. The temperature decrease and degassing of CO_2 should not affect the surface properties/secondary precipitate formation according to our previous studies.[1-2] If releasing pressure and cooldown induced precipitation, we would not be able to observe the different evolution of surface precipitation on the 10 mM phosphate samples from other experimental conditions, such as control, and 0.1 and 1 mM phosphate systems. In addition, we used GWB to calculate mineral saturation states in the 10 mM phosphate system after 96 h reaction after

degassing to ambient pressure and cooling down to 25 °C. The saturation states of secondary precipitates we observed (strengite, berlinite, gibbsite) decreased, indicating lower precipitation potential. There is a caveat using a 0.2 µM syringe filter because it may not remove nanoscale amorphous particulates from the solution. However, we can still conclude that a higher concentration of phosphate promotes biotite dissolution and that phosphate enhances secondary precipitation of Fe- and Al-containing minerals. The formation of amorphous particulates consumed cations released from biotite dissolution, leading to lower aqueous cation concentrations. If we can successfully remove all the secondary precipitates in the solution, then the concentrations measured by ICP-OES will be the net results of dissolution and precipitation. However, if there are residual amorphous particles in the solution after filtration, the redissolution of these particles during acidification for ICP-OES sample preparation will cause higher ion concentration than the net concentrations of dissolution and precipitation, which are closer to the concentrations released from dissolution. Nevertheless, the slightly higher concentrations in ICP-OES results can still support our conclusions on the concentration-dependent and element-specific effects of phosphate.

Thermodynamic calculations:

The initial pH was calculated by GWB (Geochemists' Workbench, Release 8.0, RockWare, Inc), and the thermo.com.V8.R6+.dat database was chosen for the calculation. In the database, the B-dot equation was used to calculate the activity coefficients of the aqueous species at high ionic strength. The fugacity of 102 atm CO_2 was recalculated to be 76.5 atm using Duan and Sun's equation.[3] Under our experimental conditions (1 M NaCl at 95 °C and 102 atm of CO_2), the initial pH was around 3.16.

The pH values after 22 h and 96 h reactions were calculated by taking the ICP-OES and IC results as the input for GWB calculations (Table S2). In this calculation, we assumed that the concentration of Cl^- did not change much, but the loss of the Na^+ equals to the release of K^+ because of cation-exchange reactions between Na^+ and biotite interlayer K^+. Then the cation activities, pH values, and saturation ratios of minerals were obtained. The pH values and saturation ratios of the possible secondary minerals observed by TEM and SEM are shown in Table S2. Although, based on the calculations, illite was undersaturated, fibrous illite formed on the biotite surface in all three reaction systems. Hu et al.[4] discussed that illite might be locally saturated near the biotite surface

due to concentration and pH gradients existing between surface and bulk solution in stationary batch reactor systems. Additionally, lower ion concentrations would be required for heterogeneous nucleation of fibrous illite on a biotite surface than for the homogeneous nucleation calculated by GWB. Although the saturation ratios for gibbsite were slightly negative in the 1 mM phosphate system, it could still form on the biotite surface because of the same reasons as for illite formation. However, there is a caveat in the saturation indices obtained from GWB calculations by taking the ICP-OES results as input. The ICP-OES results show the net cation concentrations of dissolution and secondary precipitation. The calculated indices reflect the saturation states after precipitation, and thus are lower than those of the systems starting to precipitate. Nonetheless, the trends of the saturation indices in different systems with different phosphate concentrations and after different reaction times should be same.

Thermodynamic prediction for 20 µM phosphate system:

To predict mineral saturation states for 20 µM phosphate system (a commonly found phosphate concentration in field sites), GWB calculations were conducted by taking the aqueous cation concentrations obtained in the 1 mM phosphate reaction system as inputs. This assumption of cation concentrations is reasonable because in 1 mM phosphate system, the aqueous Mg and Si concentrations are essentially similar to those in the control (Figure 1), the concentrations of Mg and Si in the 20 µM system should be close to both in the 1 mM phosphate and control systems. In addition, the aqueous Fe and Al concentrations might be higher in 20 µM system than in 1 mM phosphate system due to the more secondary precipitation of Fe- and Al-containing minerals in a higher concentration of phosphate system. Using the cation concentrations in the 1 mM phosphate can predict the minimum mineral saturation states in the 20 µM phosphate system, indicating the precipitation potential. The calculation results are also shown in Table S2. Strengite is saturated with just 20 µM phosphate, indicating that even very lower phosphate concentrations can promote secondary precipitation of Fe- and Al-containing minerals. The lower mineral saturation states with 20 µM phosphate than 1 mM and 10 mM phosphate systems could confirm our assumption that the extent of secondary precipitation is lower for 20 µM than 1 mM phosphate.

In-situ **pH measurements:**

A special pH probe (Corr Instrument, San Antonio, TX) was calibrated and used to measure *in-situ* pH at 95 °C and 102 atm of CO_2. The method of pH probe calibration was modified from

Shao et al.[1] The probe was calibrated at 95 °C under room pressure in 1 M NaCl solution with different pH values, adjusted under ambient conditions. Shao et al. reported that pressure within 1-102 atm does not affect the calibration. The pH of the calibration solutions at 95 °C was calculated using GWB. After recording the potential of the pH probe at different pH solutions, a calibration curve could be obtained to link potential with pH values at 95 °C. During pH measurements, the probe was put inside the reactor, where 25 pieces of biotite flakes were reacting in 100 mL of 1 M NaCl solution. This solid to liquid ratio was the same as in the batch dissolution experiments. The *in-situ* pH measured after 96 h reaction was 3.3, close to the GWB calculated pH value.

Table S2 Calculated pH values and saturation indices with respect to potential secondary mineral phases after 22 and 96 h reaction time

	22 h		96 h	
	pH	**Mineral saturation states (log Q/K)**	**pH**	**Mineral saturation states (log Q/K)**
Control	3.27	Goethite: 5.47; Gibbsite: -0.11; Illite: <-3	3.43	Goethite: 6.41; Gibbsite: 0.73; Illite: -1.9
1 mM phosphate	3.24	Strengite: 3.07; Berlinite: 0.67; Gibbsite: -0.74; Illite: <-3	3.30	Strengite: 3.4; Berlinite: 0.9; Gibbsite: -0.5; Illite: <-3
10 mM phosphate	3.31	Strengite: 4.63; Berlinite: 2.3; Gibbsite: -0.04; Illite: <-3	3.52	Strengite: 5.0; Berlinite: 2.4; Gibbsite: .2; Illite: -0.1
20 µM phosphate	3.24	Strengite: 1.38; Gibbsite: -0.72; Diaspore: 0.06; Illite < -3	3.31	Strengite: 1.8; Gibbsite: -0.42; Diaspore: 0.36; Illite: < -3

Dissolution of K:

The concentrations of K^+ in the solutions were almost the same for all reaction systems (0, 0.1, 1, and 10 mM phosphate) after biotite dissolution at any measurement time within 96 h. The release of K^+ is mainly through ion-exchange reactions with H^+ or Na^+ in the solution. The ionic strength

of the reaction solutions was controlled to be about 1.0 M NaCl. In addition, the final pH values (96 h) of the reaction systems simulated by GWB were 3.43, 3.30, and 3.52 for the control, 1 mM phosphate, and 10 mM phosphate systems, respectively (Table S2). Therefore, we suggest that the similar concentrations of aqueous K^+ observed in the three systems resulted from similar extents of ion-exchange reactions occurring.
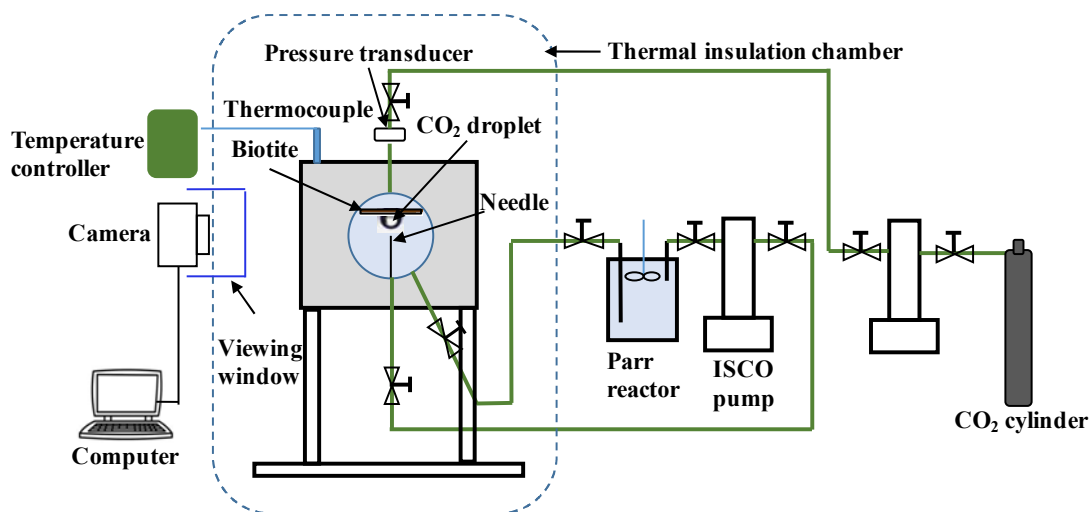
S3. Contact angle measurements

Figure S2 Apparatus for high temperature and high pressure contact angle measurements. Reprinted with permission from Zhang, L.; Kim, Y.; Jung, H.; Wan, J.; Jun, Y.-S., Effects of Salinity-Induced Chemical Reactions on Biotite Wettability Changes under Geologic CO_2 Sequestration Conditions. *Environmental Science & Technology Letters* **2016**, *3*, 92-97. Copyright (2016) American Chemical Society.

Contact angles measured under ambient conditions:

Under ambient conditions with DI water, using a contact angle analyzer (Surface Electro Optics, Phoenix 300), contact angles were measured for biotite samples reacted in control (A), 0.1 mM (B), 1 mM (C), and 10 mM (D) phosphate systems at 95 °C and 102 atm of CO_2 for 70 h (Figure S3). The absolute values of the ambient condition contact angle can be different from those obtained at high temperature and CO_2 pressure. However, based on our prior testes, the general trend of contact angles among the biotite samples reacted in different phosphate systems should be the same.

Contact angles measured under high P/T:

The captive drop method was used to measure both static and dynamic contact angles (CA) in a high temperature and high pressure setup (Figure S2). The reacted biotite flake was horizontally mounted to a stainless-steel plate inside the upside down chamber. The chamber was filled by CO_2-saturated brine, equilibrated with $scCO_2$ at a pressure of 102 atm. The temperature was maintained at 48 ± 1 °C during the measurements. For static CA measurements, a $scCO_2$ droplet was generated and released onto the biotite basal surface through the tip of the needle connected to a syringe pump. The status of the droplet on biotite surface was imaged with high-resolution time-lapse camera (6.2 Megapixel, Nikon D7000). For dynamic CA measurements, the tip of the needle was located closer to mineral surface than for static CA measurements. The volume of the $scCO_2$ droplet at the tip of the needle contacting the mineral surface was controlled by the syringe pump. When the volume of the $scCO_2$ droplet was increasing (CO_2 advancing), the water phase was retreating (water receding) driven by the inflating of the $scCO_2$ bubble. By the same token, when $scCO_2$ was receding, the water phase was advancing. This process was recorded by the camera.

After the measurements, the obtained images were analyzed using ImageJ software, combined with DropSnake and LowBond Axisymmetric Drop Shape Analysis (LB-ADSA) plugins. As a convention, the water contact angles ($CA_{H2O} = 180° - CA_{CO2}$) were reported. During dynamic CA measurements, when the highest $scCO_2$ contact angle was reached, the water contact angle was reported as the receding contact angle. During $scCO_2$ receding, at the lowest $scCO_2$ contact angle, the water contact angle was reported as the advancing contact angle. The contact angle hysteresis value is generally expressed as the difference between the advancing and receding contact angles. For some samples, even though the $scCO_2$ droplet was withdrawn through the connecting pump, $scCO_2$ disconnected from the needle tip and adhered to the mineral surface ($scCO_2$ adhesion).

A. Ambient condition contact angle

B1. High P/T contact angle   **B2. High P/T dynamic contact angle**
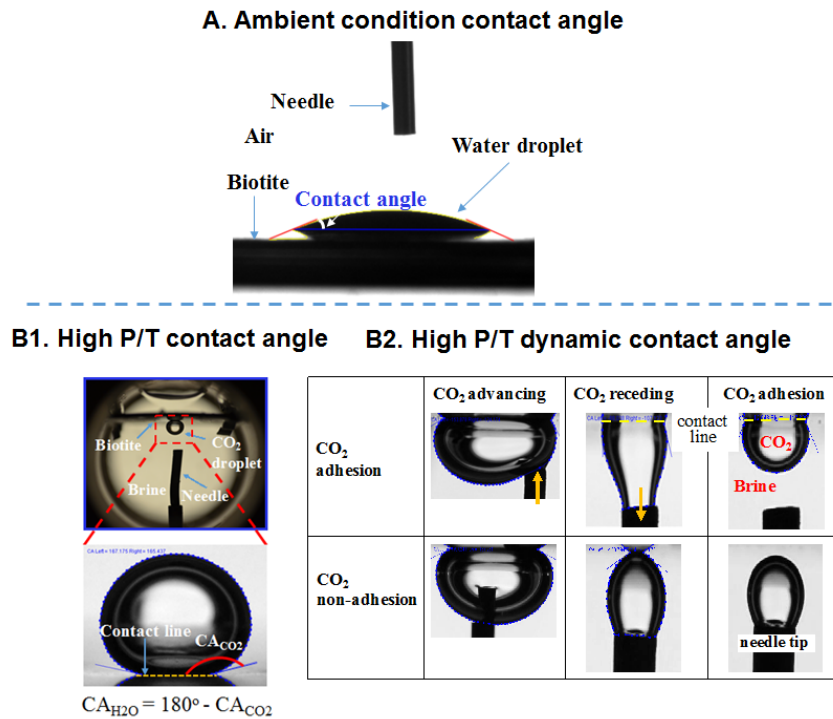
$CA_{H2O} = 180° - CA_{CO2}$

Figure S3 (A) Image taken during ambient condition contact angle measurements. (B) Contact angle measurement process under high P/T conditions.

Effects of secondary minerals on wettability alteration:

Strengite, berlinite, and gibbsite were identified on the biotite surface after reaction with 10 mM phosphate. While hydrophilicity information for strengite or berlinite is not available, a previous report found that a gibbsite surface is much more hydrophilic than a siloxane surface.[5] Therefore, if gibbsite is a secondary mineral phase, it will make the exposed surface more hydrophilic than a siloxane-terminated biotite basal surface.[6] Without knowing strengite or berlinite hydrophilicity information, we cannot determine whether the precipitation of different phases is the most dominant mechanism changing the surface wettability. Nevertheless, the coating of gibbsite on the biotite surface can be a factor enhancing the surface hydrophilicity.

S4. Aqueous complexation

Aqueous solutions after reaction for 22 h in control, 0.1 mM, 1 mM, and 10 mM phosphate systems were filtered through a 0.2 μm membrane and measured by UV-Vis. Figure S4 shows a peak around 275 nm for all spectra. It has been reported that both $FeOH^{2+}$ and $FeH_2PO_4^{2+}$

complexes contribute to the absorbance at 275 nm.[7] The difference in absorbance from the four systems was not discernible with a low value around 0.05, indicating the $FeH_2PO_4^{2+}$ complex amount was very small in the phosphate systems. Hence, aqueous complexation in the phosphate systems is not the main mechanism affecting biotite dissolution.
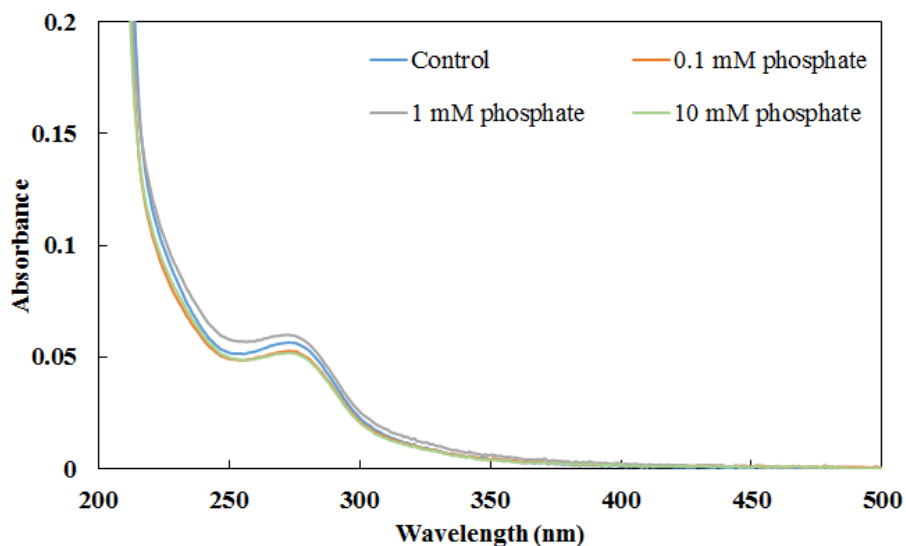

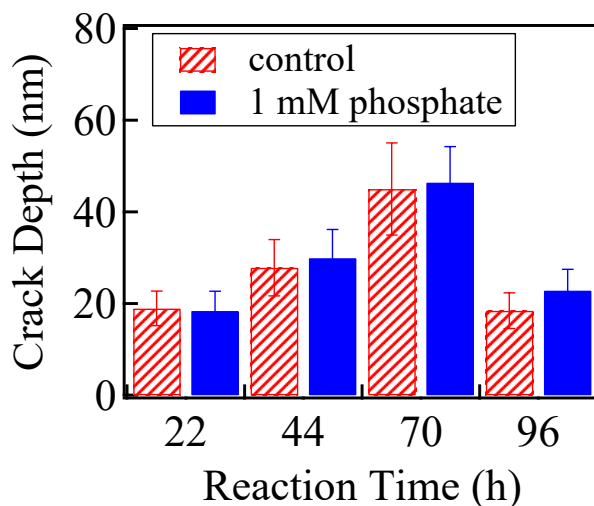**Figure S4** UV spectra of reacted solutions

S5. Analyses of crack depth

Figure S5 Average depths of cracks formed on biotite basal surfaces after reaction. The depth was taken from the average of the depths of 80 spots from four representative AFM images obtained from the reacted samples.
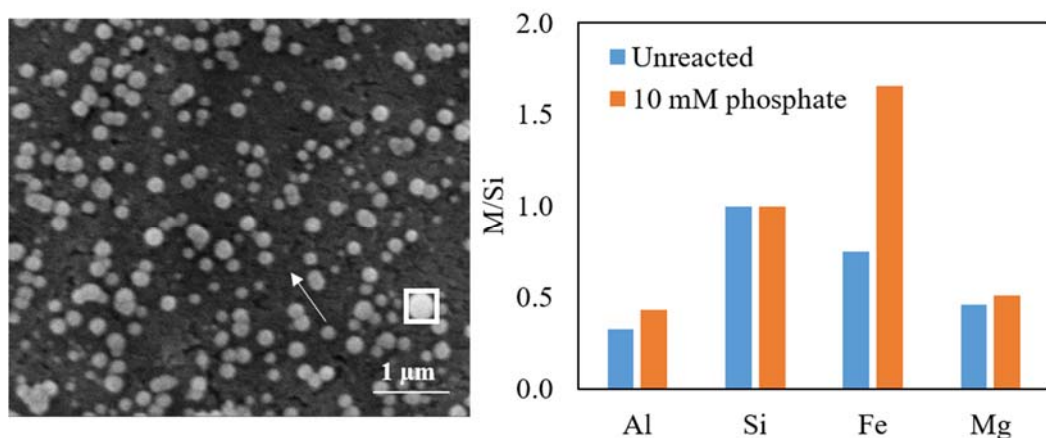
S6. SEM measurements

Figure S6 SEM observations of biotite basal surface after reaction at 95 °C and 102 atm of CO_2 for 70 h with 10 mM phosphate. On the left is an SEM image of the reacted basal surface, and on the right are the EDX results of the particle formed with 10 mM phosphate, indicated by the white box in the left image, and unreacted biotite (SEM image not shown). M/Si is the Si weight percent-normalized element content. The white arrow in the left image points to the thin film of amorphous phases.

S7. HR-TEM measurements: EDX results

A. 22 h, solution, 1 mM

B. 22 h, solution, 10 mM

C. 22 h, surface, 10 mM
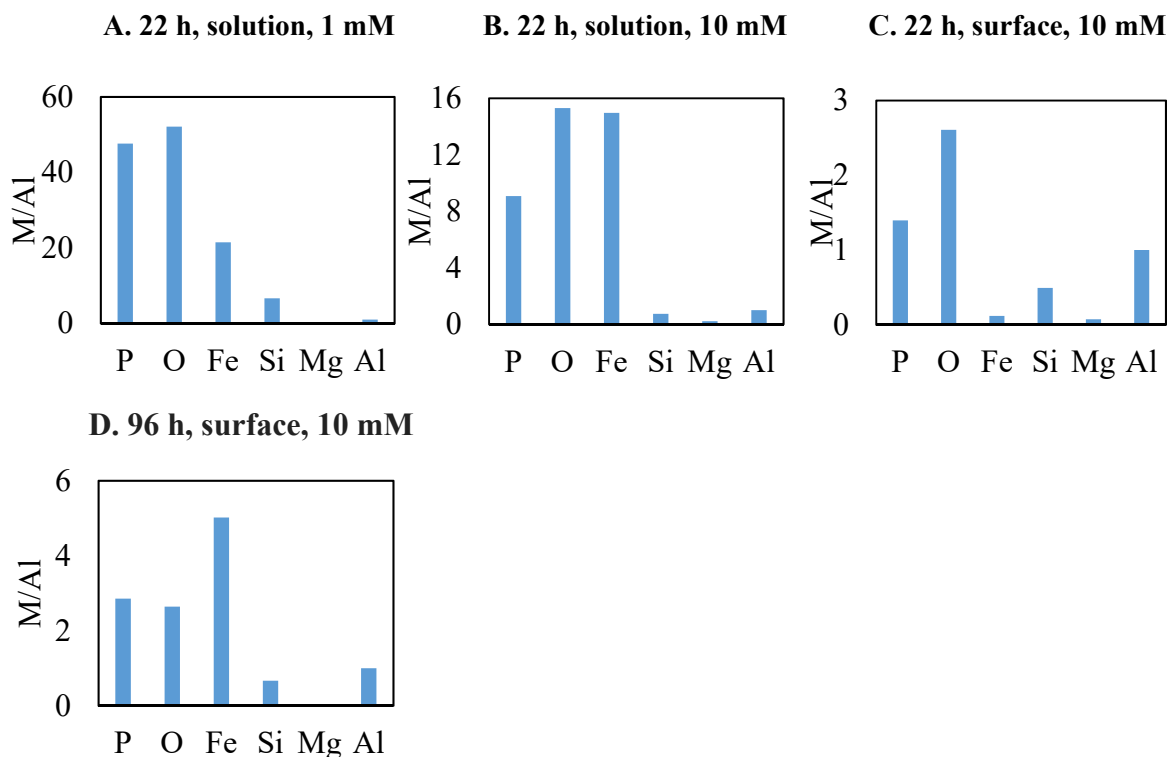
D. 96 h, surface, 10 mM

Figure S7 EDX analyses by HR-TEM of particles observed from samples: (1) taken from solutions after reaction for 22 h with 1 mM (A) and 10 mM (B) phosphate, and taken from biotite surface with 10 mM phosphate (C), (2) taken from biotite surface with 10 mM phosphate after 96 h reaction (D). The corresponding images are shown in Figure 4 in the main text. M/Al is the Al weight percent-normalized element content. For unreacted biotite, the weight ratios of different elements are O : Fe : Si : Mg : Al = 6.5 : 2.3 : 3.1 : 1.4 : 1.0.

The calculated d-spacings, 1.82 Å and 2.00 Å, matched with gibbsite[8] for particles from reacted biotite basal surfaces in both the 1 mM and 10 mM phosphate systems. Although thermodynamically the 1 mM and 10 mM phosphate systems were not supersaturated with gibbsite after 22 h reaction (Table S2), gibbsite could still form due to local supersaturation near biotite surfaces, and its heterogeneous precipitation on biotite surfaces could occur at lower ion concentrations than required for homogeneous precipitation (Detailed explanation can be found in S2). Consistently, higher amounts of Al were observed in the particles with phosphate (Figure S7).

Table S3 Analyses of d-spacings obtained from particles detached from biotite reacted with 10 mM phosphate for 96 h (corresponding to Figure 4B)

d-spacing measured (Å)	d-spacing from reference for (Å)					
	Strengite	Crystal Plane	Berlinite	Crystal Plane	Gibbsite	Crystal Plane
4.56	4.36	(2,1,0)			4.38	(1,1,0)
2.51	2.55	(1,2,3)	2.47	(1,1,0)	2.47	(3,1,-1)
1.67	1.60	(5,2,3)	1.56	(2,1,-2)	1.69	(4,0,2)
1.48	1.48	(3,5,2)	1.39	(2,0,6)	1.46	(3,3,0)
1.29			1.30	(1,0,8)		
1.00			1.16	(3,1,-2)		

S8. Residual phosphate concentrations in reaction systems

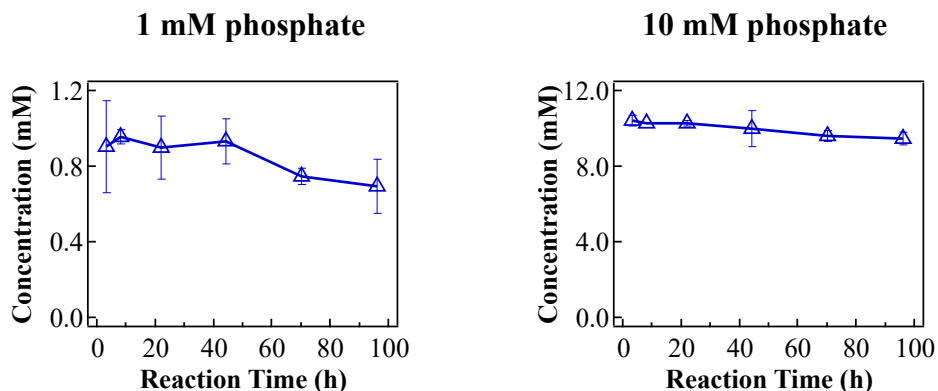**1 mM phosphate**   **10 mM phosphate**

Figure S8 Residual concentrations of phosphate in the brine at various elapsed reaction times

We used biotite flakes with dimensions of 2.0 cm × 0.8 cm, so the original biotite surface area was around 3.2 cm². After 70 h reaction, the removal of phosphate was about 0.4 mM in the 10 mM phosphate system. Because we had both homogeneous precipitation and surface precipitation, we roughly assume that 0.1 mM phosphate was removed by precipitation on the surface and that 0.05 mM strengite formed. The density of strengite is about 2.87 g/cm³. We further assumed that the thickness of surface precipitates was 200 nm, so the covered surface area would be about 130 cm², much higher than 3.2 cm². Therefore, the more than enough phosphate was removed from solution than was needed for surface coverage. This can in turn support that there is homogeneous precipitation.
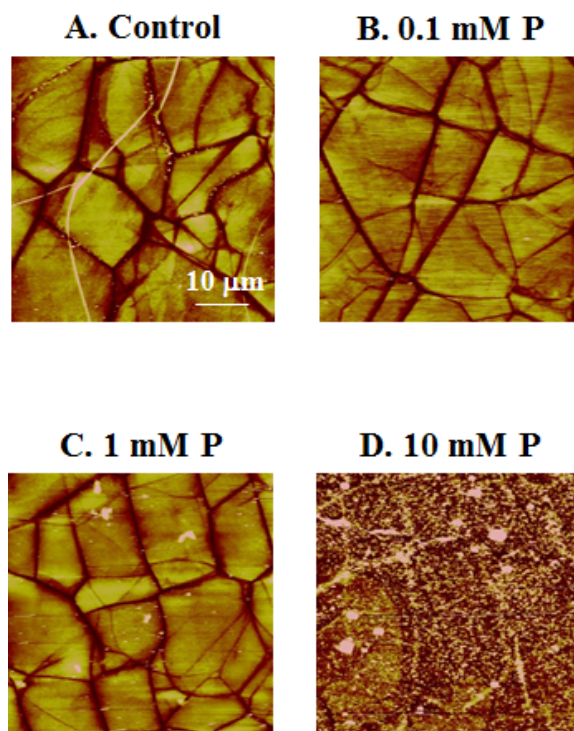
Figure S9 AFM contact mode images for biotite basal planes after 70 h reaction at T = 95 °C and P_{CO2} = 102 atm with a salinity of 1.0 M NaCl and initial pH of 3.16 without phosphate (A), with 0.1 mM phosphate (B), 1 mM phosphate (C), and with 10 mM phosphate (D).

S9. The role of CO_2

After CO_2 is injected into the system, it will dissolve into brine, forming $CO_2(aq)$, H^+, HCO_3^-, and CO_3^{2-}. The pH will decrease to about 3.16 in 1.0 M NaCl solution at 95 °C and 102 atm of CO_2. At the low pH, the main component of dissolved species will be $CO_2(aq)$, but the concentration of carbonate will be lower than 1e-8 molal under our experimental conditions. Our previous report[9] revealed that bicarbonate complexation effects on biotite dissolution were minor under the experimental conditions (1 M NaCl, 35–95 °C and 75–120 atm CO_2). However, the CO_2 molecules in brine could get into the biotite interlayer and promote biotite surface cracking.[9] In the current study, we maintained the same temperature and pressure for all three reaction systems (control, 1 mM phosphate, and 10 mM phosphate). Therefore, the differences of the results came from the presence of different phosphate concentrations. CO_2 plays an important role in biotite dissolution but is not responsible for the different results observed for the three reaction systems.

S10. Formation of fibrous illite

Generally, biotite dissolves according to the following chemical equation:[9]

$$K(Mg, Fe)_3AlSi_3O_{10}(OH, F)_2 + H^+ \rightarrow K^+ + Mg^{2+} + Fe^{2+} + Fe^{3+} + Al^{3+} + Si^{4+} + F^- + H_2O$$
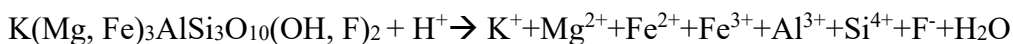
As reported in previous publications, the local dissolved ions near the biotite surface can precipitate out as fibrous illite. Additionally, fibrous illite has the same monoclinic crystal structure as biotite. There are less than 3.1% lattice mismatches between biotite and illite. There will be only a small lattice mismatch for the heteroepitaxial nucleation of fibrous illite on biotite.[4]
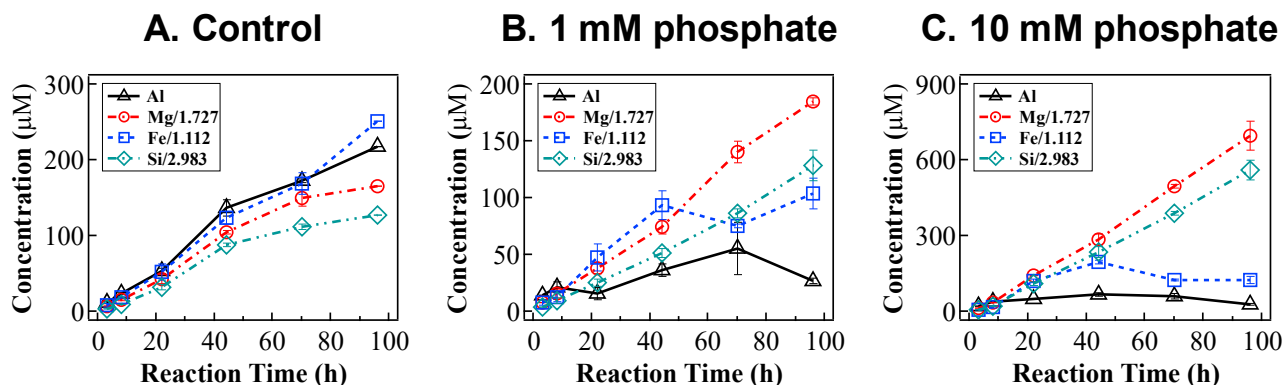
S11. Dissolution stoichiometry

Figure S10 Normalized ion concentrations by biotite chemical formula after reactions in control (A), 1 mM phosphate (B), and 10 mM phosphate (C) system at 95 °C and 102 atm CO_2.

References

1. Shao, H. B.; Ray, J. R.; Jun, Y. S., Dissolution and Precipitation of Clay Minerals under Geologic CO_2 Sequestration Conditions: CO_2-Brine-Phlogopite Interactions. *Environ. Sci. Technol.* **2010,** *44* (15), 5999-6005.

2. Zhang, L.; Jun, Y.-S., Distinctive Reactivities at Biotite Edge and Basal Planes in the Presence of Organic Ligands: Implications for Organic-Rich Geologic CO_2 Sequestration. *Environ. Sci. Technol.* **2015,** *49* (16), 10217-10225.

3. Duan, Z.; Sun, R., An improved model calculating CO_2 solubility in pure water and aqueous NaCl solutions from 273 to 533 K and from 0 to 2000 bar. *Chem. Geol.* **2003,** *193* (3), 257-271.

4. Hu, Y.; Ray, J. R.; Jun, Y. S., Biotite-brine interactions under acidic hydrothermal conditions: fibrous illite, goethite, and kaolinite formation and biotite surface cracking. *Environ. Sci. Technol.* **2011,** *45* (14), 6175-80.

5. Tenney, C. M.; Cygan, R. T., Molecular simulation of carbon dioxide, brine, and clay mineral interactions and determination of contact angles. *Environ. Sci. Technol.* **2014,** *48* (3), 2035-2042.

6. Bickmore, B. R.; Rosso, K. M.; Nagy, K. L.; Cygan, R. T.; Tadanier, C. J., Ab initio determination of edge surface structures for dioctahedral 2: 1 phyllosilicates: Implications for acid-base reactivity. *Clays Clay Miner.* **2003,** *51* (4), 359-371.

7. Wilhelmy, R. B.; Patel, R. C.; Matijevic, E., Thermodynamics and kinetics of aqueous ferric phosphate complex formation. *Inorg. Chem.* **1985,** *24* (20), 3290-3297.

8. Chichagov, A., Information-Calculating System on Crystal Structure Data of Minerals.(MINCRYST)-Kristallographiya. In *Cosultada en www. mincryst, http://database. iem. ac. ru/mincryst*, 1990; Vol. 35, pp 610-616.

9. Hu, Y.; Jun, Y. S., Biotite dissolution in brine at varied temperatures and CO_2 pressures: its activation energy and potential CO_2 intercalation. *Langmuir* **2012,** *28* (41), 14633-41.